Journal of Environmental Sciences 168 (2026) 530–537

Contents lists available at ScienceDirect

Journal of Environmental Sciences

journal homepage: www.elsevier.com/locate/jes

JES JOURNAL OF ENVIRONMENTAL SCIENCES www.jesc.ac.cn

Research Article

In situ product monitoring in heterogeneous reaction of gaseous trimethylamine on $Fe_2O_3/Fe(NO_3)_3$: Effect of environmental factor and particle property

Chenxu Gao[a], Cheng Chen[a], Jiangyao Chen[a,b,*]

[a] *Guangdong Key Laboratory of Environmental Catalysis and Health Risk Control, Guangdong Basic Research Center of Excellence for Ecological Security and Green Development, School of Environmental Science and Engineering, Guangdong University of Technology, Guangzhou 510006, China*

[b] *Guangzhou Key Laboratory of Environmental Catalysis and Pollution Control, Guangdong-Hong Kong-Macao Joint Laboratory for Contaminants Exposure and Health, Institute of Environmental Health and Pollution Control, Guangdong University of Technology, Guangzhou 510006, China*

ARTICLE INFO

Keyword:
Organic amine
Atmospheric particles
Heterogeneous reaction
In-situ monitoring
Mechanistic study

ABSTRACT

Gas-particle reactions represent an important atmospheric heterogeneous transformation process for organic amines (OAs). Environmental factors and particle properties may impact the gas-particle reaction products. Although the products from gas-particle reactions can be monitored by various *in situ* techniques, related data remain scarce. Here, the interfacial and gaseous products from the reaction of trimethylamine on $Fe_2O_3/Fe(NO_3)_3$ particles under light irradiation with mixed NO_2, O_2, SO_2 and H_2O were monitored using in-situ diffuse reflectance Fourier transform infrared spectroscopy and proton transfer reaction time-of-flight mass spectrometry. Dark reaction of gaseous trimethylamine on $Fe_2O_3/Fe(NO_3)_3$ generated two interfacial products types: N-containing ones ($CH_3N{=}CH_2$, CH_3NO_2, $(CH_3)_2NCHO$, and $CH_3N(OH)CHO$) and N-free ones (alcohols, aldehydes and acids), both accumulating with reaction progression. Light irradiation and O_2 oxidation enhanced formation of these products, while NO_2 promoted the production of CH_3NO_2 and $(CH_3)_2NCHO$. H_2O and SO_2 occupied the active sites of particles to inhibit the formation of all products. Compared to $Fe(NO_3)_3$, Fe_2O_3 showed absolute dominance in contribution to the formation of products. Considering the smaller particle size of Fe_2O_3 and excess $Fe(NO_3)_3$, the physical mixing of them reduced the generation of interfacial products. Furthermore, gaseous products of CH_3OH, HCHO, CH_3CHO, HCOOH and CH_3COOH detection clarified the N-free interfacial products. The presence of $Fe(NO_3)_3$ inhibited the formation of HCOOH and favored the formation of CH_3CHO in the gas phase. By combining product information with thermodynamic calculations, the heterogeneous reaction pathways of trimethylamine were tentatively proposed. These findings provide a guiding significance for the migration of OAs in real atmospheric environment.

1. Introduction

Organic amines (OAs) are a group of unique N-containing organics that have a great impact on global climate change, ecosystem, and human health (Duporte et al., 2016; Niu et al., 2021; Sha et al., 2021). Biological and human activities ceaselessly release OAs such as methylamine, dimethylamine, diethylamine, and trimethylamine (TMA) into atmosphere (Huang et al., 2022b; Liu et al., 2022). These OAs then become prone to homogeneous and heterogeneous reactions with various oxidants (such as free radicals, and O_3) and particulate matter (Arathala and Musah, 2021; Gai et al., 2010; Liu et al., 2017), producing new particles and promoting the formation of aerosols (Chen et al., 2019; Ge et al., 2011; Liu et al., 2017; Place et al., 2017) in the atmosphere. The rates of heterogenous reactions of OAs are always smaller than those of homogeneous reactions due to them being limited by the physical state of reactants (Levenspiel, 1972). However, given the complexity of the actual atmospheric environment, it is imperative to investigate the heterogeneous reactions between OAs and various environmental reactants (such as particles, gas, and light) and the resulting potential impact on atmospheric environment.

Atmospheric particles provide important interfaces for heterogeneous reactions of gaseous organics (Ginoux et al., 2012). As the active component in atmospheric particles, metal oxides such as Fe_2O_3, TiO_2, CeO_2, and Co_3O_4 have been reported to adsorb OAs and other organics through active sites to initiate protonation or coordination reactions (Helali et al., 2011; Lien et al., 2005; Wang et al., 2020; Zhang et al., 2013; Zhao et al., 2020). Under light irradiation, metal oxides exhibited efficient catalytic activity towards organics (Styler and Donald-

* Corresponding author. .
E-mail address: chenjiangyao@gdut.edu.cn (J. Chen).

https://doi.org/10.1016/j.jes.2026.01.012
Received 10 September 2025; Received in revised form 4 January 2026; Accepted 4 January 2026
Available online 7 January 2026
1001-0742/© 2026 The Research Center for Eco-Environmental Sciences, Chinese Academy of Sciences. Published by Elsevier B.V.

son, 2012). In addition to metal oxides, inorganic salts such as nitrate and sulfate were also found acting as important components on atmospheric particles (Li et al., 2006). While OAs show alkaline characteristics, they are prone to acid-base neutralization reaction with the inorganic salts. For example, dimethylamine has been reported to react with nitrate to form ammonium nitrate (Sorooshian et al., 2008). Therefore, both metal oxides and inorganic salts affect the heterogeneous reaction of OAs on atmospheric particles through various reactions such as acid-base neutralization and photocatalytic reactions.

Furthermore, the presence of other environmental gases such as NO_2, O_2, SO_2, and H_2O may also affect the heterogeneous reaction of OAs on atmospheric particles. It has been reported that O_2 and NO_2 promote the formation of organic aerosols (Chu et al., 2016; Liu et al., 2012), while under light irradiation, H_2O generates •OH to further oxidize organics (Grassian, 2001). Moreover, SO_2 competes with propylene and organic acids for active sites on TiO_2 (Chu et al., 2019) and Fe_2O_3 (Wu et al., 2013; Yang et al., 2020). The competitive reactions on these metal oxides generally inhibit the heterogeneous transformation of organics. However, in the case of the coexistence of mixed environmental gases, the promotion or inhibition of the reaction may happen at the same time (Chen et al., 2023; Zheng et al., 2022). For example, SO_2 competes with acetic acid for the active sites on Al_2O_3 and $CaCO_3$ (Yang et al., 2020), however, the addition of H_2O and NO_2 breaks the competition by promoting the conversion of SO_2 to sulfate (Wang et al., 2022). Clearly, not just metal oxides and inorganic salts present on atmospheric particles, but also light irradiation and other environmental gases play an important role in heterogeneous reactions of gaseous organics such as OAs on particles. However, research focusing on the products of heterogeneous reaction and the reaction pathways of OAs on atmospheric particles in the presence of complex environmental gases is scarce in literature.

In the present study, the chemicals of TMA, Fe_2O_3, and $Fe(NO_3)_3$ were selected as a model OA, a metal oxide, and an inorganic salt, respectively. The heterogeneous reaction of TMA on $Fe_2O_3/Fe(NO_3)_3$ was investigated with the presence of individual (single) and mixed environmental gases (NO_2, O_2, SO_2, and H_2O) under dark and light conditions. The in-situ diffuse reflectance Fourier transform infrared spectroscopy (DRIFTs) and proton transfer reaction time-of-flight mass spectrometry (PTR-TOF-MS) were used to monitor the interfacial and gaseous products during the reaction. Effects of various environmental factors and properties of particles on the formation of products were discussed. After combining the information about products with density functional theory (DFT) calculations, the heterogeneous reaction pathways of TMA were proposed. The coupled DRIFTs and PTR-TOF-MS in-situ detection method was employed in this study. This methodology enabled simultaneous tracking of interfacial products on particles and volatile reaction products in the gas phase under complex gas mixtures, providing unique insights into how mixed gases and particle properties synergistically regulating TMA reaction pathways.

2. Materials and methods

2.1. Methodology

A total of 14 experiments (number as E_1, E_2, E_3, …. E_{14}) were conducted for the heterogeneous reaction of TMA on the prepared $Fe_2O_3/Fe(NO_3)_3$ particles (**Appendix A Table S1, Figs. S1 and S2**). In a typical experiment (E_{10}), a mixed gas of TMA (20 ppm), NO_2 (50 ppm), SO_2 (50 ppm), and dry air with a volumetric ratio of 1.6:1:1:0.4 (respectively) was continuously introduced at a flow rate of 40 mL/min into an *in situ* infrared cell containing 60 mg of $Fe_2O_3/Fe(NO_3)_3$. The relative humidity of the mixed gas was about 40 %. A xenon lamp with an average intensity of 205 mW/cm^2 (PLS-SXE300+, Beijing Perfectlight Technology Co., Ltd., China) was used to simulate the solar light and irradiate the particles for 30 min. The organic functional groups of TMA and its conversion products on the particles were monitored using DRIFTs (Thermo Fisher Nicolet iS10, Thermo Fisher Scientific, USA). Meanwhile, the outlet gas during the reaction was collected and diluted with pure N_2 before detection by PTR-TOF-MS (PTR-TOF-MS 1000, Ionicon Analytik GmbH, Austria). Details about the preparation of particles and different characterization methods used in the current work are presented in **Appendix A Text S1**.

2.2. Theoretical calculations

Reaction energy profiles and transition states (TS) were computed using the Materials Studio 2020 DMol^3 module. All structures were optimized with the PBE functional and DNP 4.4 basis set (cutoff: 4.5 Å). Initial TS searches employed the LST/QST method, followed by NEB refinement (8 images; force convergence: 0.05 eV/Å). Moreover, TS candidates were confirmed by single imaginary frequencies and IRC analysis.

3. Results and discussion

3.1. Identification of interfacial products by DRIFTs

The reaction of TMA on $Fe_2O_3/Fe(NO_3)_3$ for 30 min was studied under dark conditions (E_1) and the interfacial products were monitored by DRIFTs. No bands were observed for pure $Fe_2O_3/Fe(NO_3)_3$, whereas after injecting TMA for 5 min, several bands within the range of 800–3500 cm^{-1} appeared. With the progress of reaction to 10 and 30 min, the intensities of all bands gradually increased, confirming the occurrence of the interfacial reaction of TMA on $Fe_2O_3/Fe(NO_3)_3$ under dark conditions (Fig. 1a).

The bands within the ranges of 2700–3500 cm^{-1} and 1900–2600 cm^{-1} belonged to C-H stretching vibration and the vibration of CH_3 groups (Murphy et al., 1993), respectively. Meanwhile, most of the bands within the range of 800–1300 cm^{-1} were attributed to N-containing group (the NC_3 band at 1044 cm^{-1} and ν_s(C-N) band at 870, 912, 935, and 1269 cm^{-1}) (Durgaprasad et al., 1972; Ge et al., 2016; Gurajala et al., 1971; Murphy et al., 1993). The gradually enhanced intensities of above bands along with reaction time revealed the adsorption and accumulation of either TMA or its conversion products on $Fe_2O_3/Fe(NO_3)_3$. The bands at 1354, 1394 and 1684 cm^{-1} were attributed to ν_s(C-O), δ(O-H) (Busca et al., 1987; Ge et al., 2016; Pettersson et al., 1997) and ν_s(C=O) (Ge et al., 2016), respectively, indicating the formation of oxidized products on particles. The appearance of C=N (935 and 1658 cm^{-1}) and NCO groups (830 cm^{-1}) also confirmed the occurrence of the reaction. These results indicated that TMA was converted to various organic products on $Fe_2O_3/Fe(NO_3)_3$ particles under dark conditions.

Previous studies have demonstrated that trace or organic gases bonded onto the surfaces of various mineral particles (such as α-Fe_2O_3) in the dark react with active species such as active oxygen and •OH (Chen et al., 2023; Golay et al., 2022). The former mainly originated from the adsorption of O_2 on the surface of mineral particles, while the latter may arise either from the redox cycle of metal's valence (Fe^{3+}/Fe^{2+}) or from the decomposition of H_2O adsorbed on the surface (Guan et al., 2014; Ma et al., 2023). As shown in **Appendix A Fig. S3a**, the $Fe_2O_3/Fe(NO_3)_3$ particles primarily consisted of Fe^{3+}. However, the presence of satellite peaks in the XPS spectrum suggested that Fe^{3+} may be locally reduced to Fe^{2+} during the preparation process (Dong et al., 1998). Additionally, as shown in **Appendix A Fig. S3b**, the $Fe_2O_3/Fe(NO_3)_3$ particles contained three types of reactive oxygen species: surface adsorbed oxygen, lattice oxygen and NO_3^- (Cao et al., 2002; Cheng et al., 2017). The appearance of O-containing functional groups such as C=O, C–O, and OH provides spectroscopic evidence for the involvement of active sites and reactive oxygen species (ROSs) in the heterogeneous reaction of TMA on $Fe_2O_3/Fe(NO_3)_3$. As reported by Xu et al. (2011), active sites and ROSs at the interfaces of mineral particles can initiate heterogeneous reactions of gaseous organic compounds, which is consistent with the observations made in the current work.

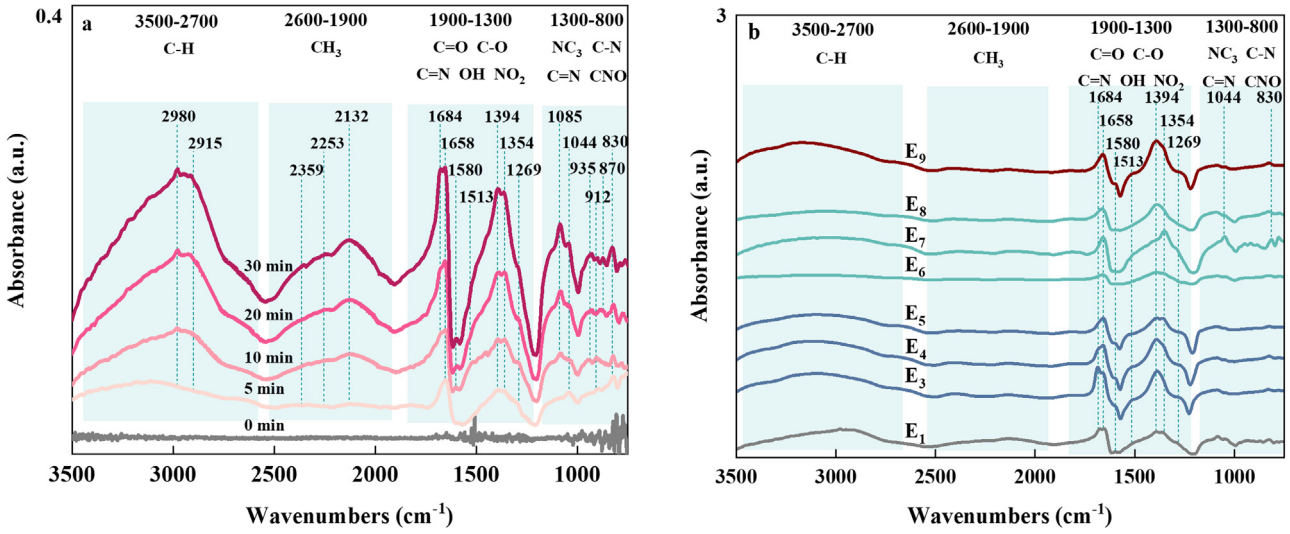


Fig. 1 – DRIFTs plot of heterogeneous reactions of TMA on particles. (a) 30 min plot of E_1, and (b) effects of NO_2, O_2, SO_2, and H_2O.

Moreover, DRIFTs results indicated that dark reaction of TMA on Fe_2O_3/$Fe(NO_3)_3$ particles generated nine main functional groups (C-H, CH_3, C-N, NC_3, C=N, O-C-O, C=O, O-H and NO_2). After comparing these groups with those reported in previous works (**Appendix A Table S2**), four N-containing products were identified including $CH_3N{=}CH_2$, CH_3NO_2, $(CH_3)_2NCHO$, and $CH_3N(OH)CHO$ along with some O-containing organic products. Although Ge et al. (2016) reported similar N-containing products during O_3 oxidation of TMA on various inorganic salts and also proposed the formation of HCHO and HCOOH from these compounds through either oxidation or hydrolysis reactions, their reaction relied on O_3 as the primary oxidant. Nevertheless, the heterogeneous reaction of TMA on Fe_2O_3/$Fe(NO_3)_3$ described in this section occurred under dark and ambient atmosphere-free conditions, primarily driven by the synergistic action of inherent ROSs (O_{latt}, O_{ads}, and NO_3^-) and active sites (Fe^{3+}) at the interface of mineral particles. This unique synergistic mechanism, which is distinct from the inorganic salt-dominated systems, may explain the broader range of products observed in the present study (such as alcohols, aldehydes, and acids, as indicated by the presence of C-H, CH_3, O-H, and C=O bands) than those reported in Ge et al. (2016).

In summary, *in situ* DRIFTs provides compelling evidence for the dark heterogeneous conversion of TMA on Fe_2O_3/$Fe(NO_3)_3$, yielding complex oxygenated and nitrogenous products. Critically, the formation of carbonyl (C=O) and other O-containing functional groups points to a reaction mechanism driven by the synergistic action of ROSs (O_{latt}, O_{ads}, and NO_3^-) and Fe^{3+} active sites. The observed reaction pathways, which are distinct from those reported for inorganic salt systems, likely enable a broader range of products from TMA. Further identification of N-free products was conducted by analyzing volatiles using PTR-TOF-MS.

3.2. *Effect of key atmosphere gases on the interfacial products*

To investigate the effect of key atmosphere gases on the interfacial products, NO_2, O_2, SO_2, and H_2O were sequentially introduced into E_1. Compared to pure TMA (E_1), the introduction of NO_2 (E_3) exhibited significant differences in the spectral band (Fig. 1b **and Appendix A Fig. S4a**). More specifically, the intensity of bands associated with CH_3 groups (1900–2600 cm^{-1}) decreased, while the intensities of bands for C-N, C=N, NO_2, C-O, C=O, and O-H groups (1269, 1354, 1394, 1513, 1580, 1658, 1684, and 1835 cm^{-1}) increased. Concurrently, the multiplet peaks within the range of 1300–1580 cm^{-1} were turned into a shoulder peak. This indicated that NO_2 participated in the interfacial reaction of TMA on Fe_2O_3/$Fe(NO_3)_3$ particles, leading to a decrease in the content of TMA and an enhanced formation of TMA derivatives including $CH_3N{=}CH_2$, CH_3NO_2, and $(CH_3)_2NCHO$, as well as various alcohols, aldehydes, and acids. This was attributed to NO_2 acting as an oxidant, and facilitating such reactions (Taylor et al., 1980; Usher et al., 2003; Wollenhaupt and Crowley, 2000). Upon simultaneous introduction of NO_2 and O_2 (E_4, Fig. 1b **and Appendix A Fig. S4b**), the spectral features remained largely consistent with those of E_3, though with slight variations in the 1300–1900 cm^{-1} region. Notably, the intensity of δ(O-H) band (1394 cm^{-1}) increased, whereas that of ν(C=O) band (1684 cm^{-1}) decreased. This suggested that the oxidative properties of O_2 were involved in both the formation of oxygenated derivatives of TMA (alcohols, aldehydes, and acids) and their subsequent oxidative product ($(CH_3)_2NCHO$), which was in line with its known function in atmospheric chemistry (Chebbi and Carlier, 1996; Hoque and Kawamura, 2016; Li et al., 2010; Usher et al., 2003). When H_2O was added to NO_2 and O_2 system (E_5, 40 % relative humidity (RH)), the intensities of all spectral bands decreased compared to those of E_3 and E_4 (Fig. 1b **and Appendix A Fig. S4c**). Among them, the δ(O-H) band (1394 cm^{-1}) was significantly reduced, while the ν(C=O) band (1684 cm^{-1}) almost disappeared, indicating that H_2O inhibited the reaction of TMA on particles. It is widely known that H_2O gets physically adsorbed onto the mineral surfaces, and competed with other gases to be adsorbed on the active sites at the mineral interface (Gao et al., 2024). The contact angle measurements further revealed that both H_2O and TMA were rapidly absorbed by Fe_2O_3/$Fe(NO_3)_3$ (contact angle of around 0°), confirming the material's strong hydrophilicity and affinity for TMA (**Appendix A Fig. S5**). This characteristic may lead to competitive adsorption of H_2O and TMA molecules for active sites on the surface of Fe_2O_3/$Fe(NO_3)_3$ when both gases are present, consequently suppressing the heterogeneous reactivity of TMA on Fe_2O_3/$Fe(NO_3)_3$.

However, the introduction of only SO_2 (E_6) to pure TMA system caused a general weakening of all spectral peaks compared to those observed in E_1 (Fig. 1b **and Appendix A Fig. S4d**). The bands for CH_3 groups and C-H stretching (1900–3500 cm^{-1}) almost disappeared, while those for C-O, O-H, C-N, NO_2, C=N, and C=O (800–1900 cm^{-1}) were significantly attenuated. This suggested that SO_2 also inhibited the reaction of TMA, which was likely due to the competition for active sites on the surface of Fe_2O_3/$Fe(NO_3)_3$. This is due to the reason that SO_2 is adsorbed on the surfaces of iron-containing particles and reacts with reactive species such as O_2^- and •OH to form sulfite (SO_3^{2-}) and bisulfite (HSO_3^-) (Chung and Quon, 1973; Urone et al., 1968). When SO_2 coexists with organic matter, it may compete for active sites on metal oxides (Yang et al., 2021). Upon simultaneous introduction of SO_2 and O_2 (E_7),

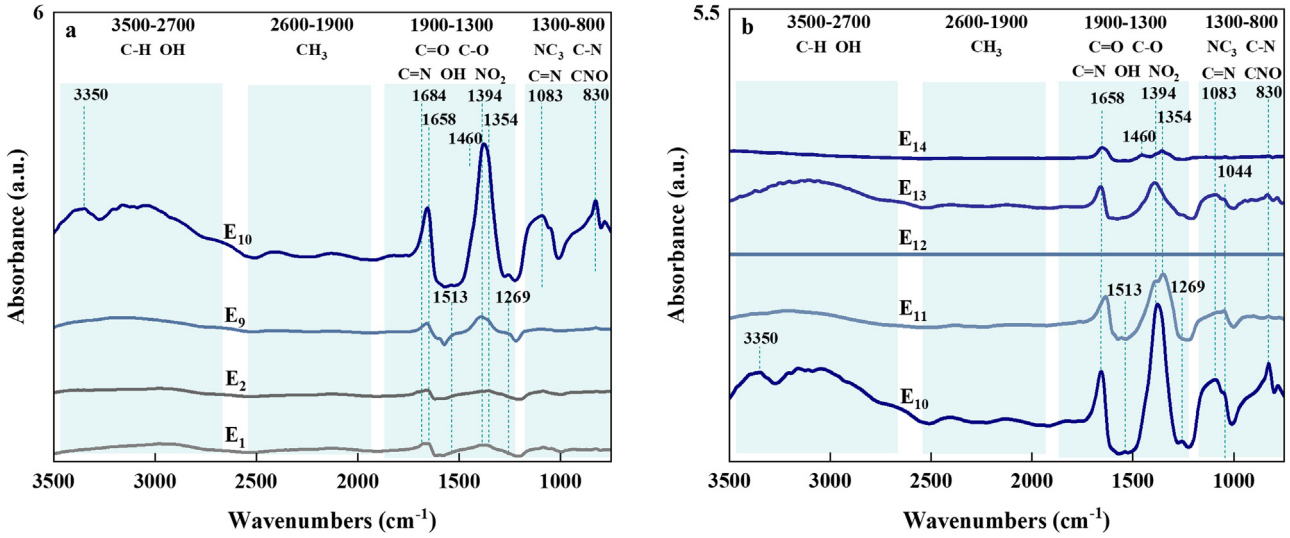


Fig. 2 – DRIFTs plot of heterogeneous reactions of TMA on particles. (a) Effects of light and (b) effects of the properties of particles.

the intensities of all spectral bands were enhanced relative to both E_1 and E_6 (Fig. 1b **and Appendix A Fig. S4e**), indicating an increased content of TMA and its derivatives at the interface. This once again demonstrated that the oxidative characteristic of O_2 not only promoted the heterogeneous reaction of TMA, but also reversed the inhibition caused by SO_2. The reversal of SO_2's inhibition by O_2 is attributable to two primary reasons: (1) the oxidation of adsorbed SO_2 to sulfate species by O_2 (Usher et al., 2002), and (2) the replenishment of reactive oxygen sites previously occupied by SO_2 (Usher et al., 2003). Consequently, the introduction of O_2 enhances the overall oxidizing capacity, mitigates the inhibitory effect of SO_2, frees the occupied active sites, and restores the reactivity towards TMA. Subsequently, adding H_2O to E_7 system (E_8) again led to the decreased intensity of all bands, reaffirming the competitive inhibitory role of H_2O (Fig. 1b **and Appendix A Fig. S4f**). Finally, when NO_2, SO_2, O_2, and H_2O were introduced simultaneously (E_9), the intensities of all spectral bands increased relative to the initial pure TMA (E_1) (Fig. 1b **and Appendix A Fig. S4g**). Further analysis revealed that the spectral characteristics in E_9 were nearly identical to those in E_4, indicating that the strong oxidizing properties of NO_2 and O_2 dominated the overall process, accelerating the heterogeneous reaction of TMA on Fe_2O_3/$Fe(NO_3)_3$ particles in a complex mixed atmosphere. The inhibitory effects of SO_2 and H_2O appeared to have mitigated, possibly because either SO_2 was oxidized to sulfate or H_2O was consumed during the enhanced oxidation of TMA, thus reducing their abilities to compete for active sites.

The complex atmospheric reactions mediated by multiple ambient gases are ubiquitous in the environment. For instance, Wang et al. (2023) demonstrated that in urban areas, declining NO_2 levels counteracted the impact of increasing O_3 on the concentration levels of nitrate radical. Similarly, He and He (2020) proposed that water enhances the O_2-driven oxidation of SO_2 on carbonaceous aerosols through autocatalytic dissociation into surface hydroxyl groups under ambient conditions. Therefore, when assessing the impacts of heterogeneous reactions on the surfaces of atmospheric particles, the prevalence of this phenomenon necessitates comprehensive consideration of complex coupling effects between ambient atmospheres and properties of particles.

3.3. Effect of light and properties of particles on the interfacial products

The impacts of light and the properties of particles (composition, and physical mixture of Fe_2O_3 and $Fe(NO_3)_3$) on the reaction of TMA on Fe_2O_3/$Fe(NO_3)_3$ were further assessed. Under light irradiation alone (E_2), the distribution of functional groups remained consistent with those under dark condition (E_1) (Fig. 2a **and Appendix A Fig. S4h**), indicating a negligible photo-driven reactivity for pure TMA. However, upon the introduction of both light and mixed gases of NO_2, O_2, SO_2, and H_2O (E_{10}), the band intensities for various products far exceeded those for all other systems (E_1-E_9) (Fig. 2a **and Appendix A Fig. S4i**). More specifically, the new band of ν_s (OH) from H_2O appeared at 3350 cm^{-1} (Pettersson et al., 1997), while the bands for other functional groups within the range of 800–1900 cm^{-1} region persisted, suggesting a potential synergistic mechanism between irradiated light and mixed gases. This synergy was attributed to the photogenerated charge carriers (e^-/h^+) on the surface of Fe_2O_3 (Kim et al., 2021) and the photolysis of $Fe(NO_3)_3$ that produced •OH (Tercero Espinoza et al., 2007), as well as e^- that reduced O_2 (Mu et al., 2017). Meanwhile, h^+ oxidized either H_2O to •OH (Chen et al., 2021) or NO_2 to NO_3^- (Sugrañez et al., 2015). In the meantime, •OH oxidized SO_2 to SO_4^{2-} (Cao et al., 2021). These radical-driven oxidative reactions consumed both SO_2 and H_2O, thereby alleviating their competitive adsorption on active sites and accelerating the oxidation of TMA. This led to an increased diversity and abundance of products including $CH_3N{=}CH_2$, CH_3NO_2, $(CH_3)_2NCHO$, $CH_3N(OH)CHO$, alcohols, aldehydes, and acids.

The composition of particles also critically influenced the heterogeneous reaction of TMA under light irradiation. When TMA reacted on pure Fe_2O_3 particles (E_{11}, removing $Fe(NO_3)_3$ from Fe_2O_3/$Fe(NO_3)_3$), the resulting infrared spectral bands were stronger than those observed in E_1-E_9, though they were weaker than those observed in E_{10} (Fig. 2b **and Appendix A Fig. S4j**). This indicated that $Fe(NO_3)_3$ acted as an active substance in Fe_2O_3/$Fe(NO_3)_3$. The reaction mechanism of $Fe(NO_3)_3$ was attributed to its poor stability under light conditions, which readily underwent photolysis to produce •OH (Gen et al., 2019; Li et al., 2018), while simultaneously facilitating the formation of oxygen vacancies and Fe^{2+} sites at the interface of Fe_2O_3. These synergistic effects enhanced the adsorption of O_2 and the transfer efficiency of electrons (e^-). The ion chromatography results proved the consumption of $Fe(NO_3)_3$ after the reaction (**Appendix A Fig. S6**). Contact angle measurements further demonstrated that the removal of $Fe(NO_3)_3$ did not compromise the initial adsorption capacity of particles for H_2O and TMA (**Appendix A Fig. S5**). Consequently, in the composite particles of Fe_2O_3/$Fe(NO_3)_3$, Fe_2O_3 serves as the primary reaction interface while $Fe(NO_3)_3$ functions as the active precursor. The removal of $Fe(NO_3)_3$ restricts the generation of •OH, diminishes the overall oxidizing capacity of the system, and reduces the yield of heterogeneous reaction products from TMA.

Given the well-established dependence of interfacial reactivity of particulate matter on its chemical composition, the present study sys-

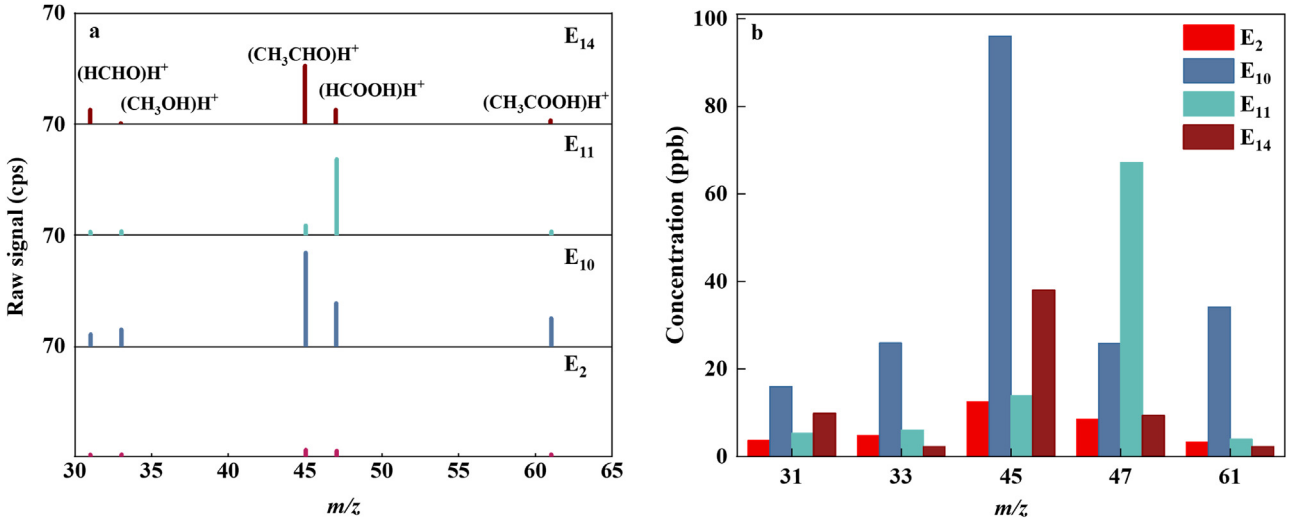


Fig. 3 – PTR-TOF-MS analysis of gaseous products of TMA on $Fe_2O_3/Fe(NO_3)_3$ particles. (a) Qualitative analysis, and (b) quantitative analysis.

tematically compares the effects of the particle size of Fe_2O_3, content of $Fe(NO_3)_3$ in the composite particulates of $Fe_2O_3/Fe(NO_3)_3$, and the configuration (composite *vs*. physical mixture) of Fe_2O_3 and $Fe(NO_3)_3$ on the heterogeneous reaction of TMA. Preparation processes and key physicochemical properties of representative samples (Fe_2O_3–50, $Fe_2O_3/Fe(NO_3)_3$–5, and Fe_2O_3+$Fe(NO_3)_3$) are detailed in **Appendix A Texts S1.1** and **S1.2**. DRIFTs analysis of E_{12} (Fe_2O_3–50, Fig. 2b **and Appendix A Fig. S4k**) revealed nearly negligible spectral signatures for TMA and its derivatives, which sharply contrasted with the experimental observations of E_{11} (100 nm) system. This indicates that both the adsorption of TMA and its subsequent surface reactivity were significantly suppressed on Fe_2O_3–50. It is proposed that the reduction in the size of solid particles may induce structural densification (Du et al., 2020; Li et al., 2019), reduce the specific surface area, diminish physisorption capacity, and lead to the loss of active sites. Consequently, while serving as the primary interface for TMA's heterogeneous reaction, Fe_2O_3 underwent deactivation.

Regarding the active component, the content of $Fe(NO_3)_3$ in $Fe_2O_3/Fe(NO_3)_3$–5 was increased while the content of Fe_2O_3 was reduced by shortening the heating time. When TMA reacted on $Fe_2O_3/Fe(NO_3)_3$–5 (Fig. 2b **and Appendix A Fig. S4l**), the types of characteristic peaks observed in the IR spectra were similar to those observed for E_{10} ($Fe_2O_3/Fe(NO_3)_3$, 10 h), however, their intensities were significantly lower than those observed in E_{10} and E_{11} (Fe_2O_3). This suggests that excessive content of $Fe(NO_3)_3$ adversely affects the reactivity of TMA. Xu et al. reported that an optimum ratio of the active component to that of the support in materials was needed to induce the synergistic effect, excessive active component may cover active sites on the material surface, and that excessive active component may cover active sites on the surface of material (Xu et al., 2008). Earlier findings from E_{11} confirm that Fe_2O_3 is the primary reactive interface for the oxidation of TMA. In $Fe_2O_3/Fe(NO_3)_3$–5, excessive $Fe(NO_3)_3$ likely masks ROSs and active sites on Fe_2O_3, while insufficient content of Fe_2O_3 may limit the number of active sites. These factors collectively impair the heterogeneous reactivity towards TMA.

In contrast, when Fe_2O_3 and $Fe(NO_3)_3$ were physically mixed (E_{14}), compared to E_{10} and E_{11}, a significant attenuation in all the spectral bands was observed (Fig. 2b **and Appendix A Fig. S4m**), indicating that simple physical mixing diminished the interfacial reactivity. Previous studies have shown that thermal treatment is employed during the preparation of multi-component materials to increase the specific surface area and exposure to active sites (Cano-Casanova et al., 2018; Liu et al., 2020). Based on this, it was speculated that in the physical mixture, $Fe(NO_3)_3$ may either block the porous structure of Fe_2O_3 or cover its existing active sites. However, $Fe_2O_3/Fe(NO_3)_3$ particles likely formed a more optimum physical interface that exposed more active sites, thereby significantly promoting the heterogeneous reaction of TMA.

In summary, environmental factors and the properties of particles synergistically influenced the heterogeneous conversion of TMA. On the one hand, light in the presence of a complex gas mixtures catalyzed the formation of reactive species (such as •OH, $•O_2^-$, and NO_x), which oxidatively consumed SO_2 and H_2O. This process alleviated competitive adsorption and accelerated the heterogeneous reaction of TMA on $Fe_2O_3/Fe(NO_3)_3$ particles. Meanwhile, properties of particles critically modulated reactivity, Fe_2O_3 served as the primary reaction interface, while $Fe(NO_3)_3$ acted as a radical precursor through photolytic generation of •OH and enhancement of oxygen vacancies/Fe^{2+} sites. The addition of $Fe(NO_3)_3$ in an optimum amount was essential, as excess amounts masked active sites or ROSs on Fe_2O_3, while insufficient amounts limited the production of radicals. Reduction in the size of particles (for example, 50 nm) induced structural densification, decreasing the surface area and active sites. Composite structuring exposed more active sites than physical mixtures, where $Fe(NO_3)_3$ either blocked pores or covered interfaces.

3.4. Qualitative and quantitative analyses of gaseous products by ptr-tof-ms

To investigate the potential for interfacial products to be released into the atmosphere, the gaseous products from E_2, E_{10}, E_{11}, and E_{14} were analyzed using PTR-TOF-MS. Five oxygenated products were identified and characterized (Fig. 3a **and Appendix A Fig. S7**): formaldehyde (*m/z* 31.014; HCHO), methanol (*m/z* 33.031; CH_3OH), acetaldehyde (*m/z* 45.031; CH_3CHO), formic acid (*m/z* 47.025; HCOOH), and acetic acid (*m/z* 61.031; CH_3COOH). No N-containing products were detected in the gas phase because the functional groups of -NH_2 and -NO_2 had strong chemisorption on the surfaces of metal oxides (Huang et al., 2022a; Ling et al., 2023), leading to their retention at the interface of $Fe_2O_3/Fe(NO_3)_3$.

In E_2, only trace amounts of CH_3CHO (4.3 ppb), HCOOH (3.7 ppb), CH_3OH (1.5 ppb), CH_3COOH (1.4 ppb), and HCHO (1.2 ppb) were generated (Fig. 3b). After introducing gases and light (E_{10}), the concentrations of CH_3CHO, HCOOH, CH_3OH, CH_3COOH, and HCHO increased to 59.5, 27.6, 11.0, 18.1, and 8.0 ppb, respectively, representing a 7–14 times increase compared to E_2. This result corroborated the synergistic oxidation mechanism involving light and environmental gases, as discussed in Section 3.3. When $Fe(NO_3)_3$ was absent (E_{11}), compared to E_{10}, the concentrations of CH_3CHO and CH_3COOH decreased by 85.5 %

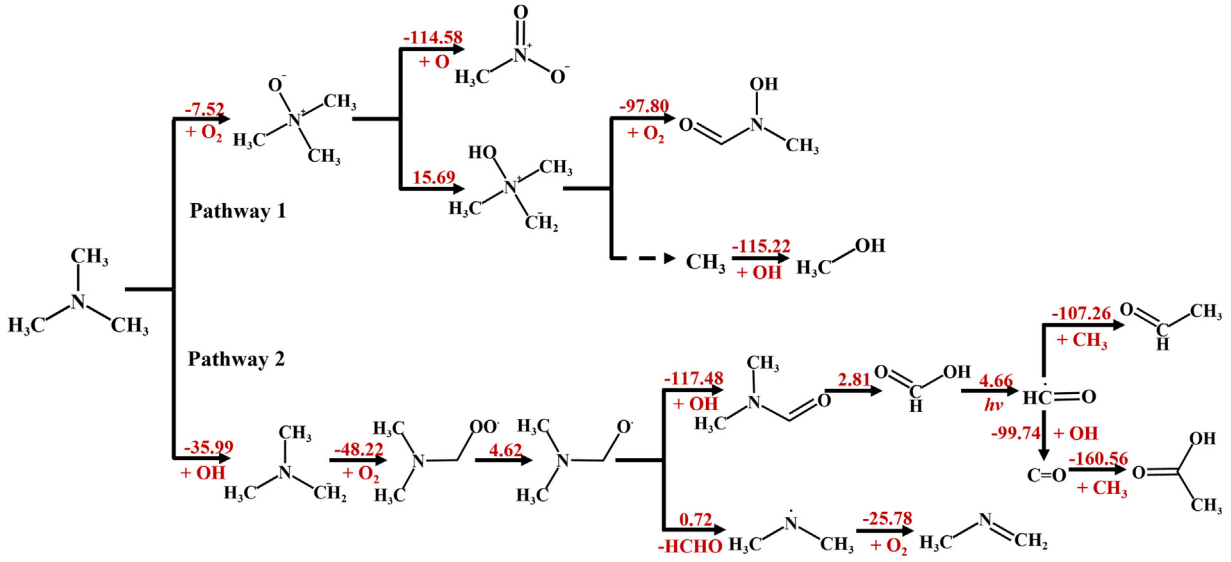


Fig. 4 – Schematic of the mechanism of heterogeneous reaction of TMA on $Fe_2O_3/Fe(NO_3)_3$ particles. Red numbers represent the reaction enthalpy (ΔE, kcal/mol).

and 88.3 %, respectively, while the production of HCOOH significantly increased by 159.5 %. This accumulation of HCOOH in the absence of $Fe(NO_3)_3$ suggested that $Fe(NO_3)_3$ was the primary adsorption and reaction interface for HCOOH. As an effective oxidant, $Fe(NO_3)_3$ had strong Lewis acid sites (ionized Fe^{3+}) (Li et al., 2024), and was capable of efficiently adsorbing molecules containing lone pairs of electrons. Therefore, HCOOH with lone pairs on both of its oxygen atoms was likely to be strongly adsorbed onto the surface of $Fe(NO_3)_3$. Compared to E_{11}, when $Fe(NO_3)_3$ was physically mixed with Fe_2O_3 (E_{14}), the concentration of HCOOH decreased by 86.1 %, while the production of CH_3CHO increased by 172.3 %. These results suggested that HCOOH may have acted as a precursor to CH_3CHO. This conclusion was consistent with the photolysis pathway of HCOOH (Wang et al., 2021; Zhang et al., 2023), where the photolysis of HCOOH produced CHO• radicals that subsequently underwent C-C coupling with CH_3 radicals to form CH_3CHO. This interfacial mediation was conclusively demonstrated through chemisorption-driven HCOOH enrichment on Fe^{3+} sites, subsequent photo-conversion of adsorbed HCOOH, and > 170 % enhanced CH_3CHO yield under interfacial (E_{14} *vs.* E_{11}). Finally, a comparison between E_{14} and E_{10} revealed that the concentrations of all five gas-phase products were lower in the physical mixture. This finding once again supported the conclusion in Section 3.3 that the integrated $Fe_2O_3/Fe(NO_3)_3$ interface was more favorable for the heterogeneous reaction of TMA.

The conversion of HCOOH to CH_3CHO observed on $Fe_2O_3/Fe(NO_3)_3$ likely represents a previously less discussed atmospheric pathway for the formation of CH_3CHO. Furthermore, the accumulation of products such as HCOOH and CH_3CHO on particles can significantly alter key physicochemical properties of the particulate matter, including hygroscopicity and efficiency to absorb light, thereby influencing the atmospheric fate of mineral dust. Moreover, under simultaneous exposure to light and ambient gases (E_{10} *vs.* E_2), the concentration of gaseous products increased by approximately 6-fold. As these oxygenated compounds are established precursors to secondary organic aerosol (SOA), heterogeneous reactions of organic amines on mineral particles under realistic atmospheric conditions likely represent a significant source for the formation of SOA.

3.5. Heterogeneous reaction pathways of TMA on $Fe_2O_3/Fe(NO_3)_3$

By integrating experimental analyses with DFT calculations, a mechanistic pathway for the heterogeneous reaction of TMA on $Fe_2O_3/Fe(NO_3)_3$ particles was proposed (Fig. 4, **Appendix A Figs. S8-S10 and Tables S3, S4**). The reaction involved two competing pathways: 1) O_2-initiated oxidation; and 2) •OH-initiated oxidation, which was determined by the environmental factors and the properties of particles. At the same time, based on the information about the products, the oxidation of N-attack and C-attack (Shen et al., 2023) sites during the heterogeneous reaction of TMA on $Fe_2O_3/Fe(NO_3)_3$ was discussed.

Initially, TMA was adsorbed on the surface of $Fe_2O_3/Fe(NO_3)_3$ through either proton transfer or acid-base interactions (Ge et al., 2016; Shen et al., 2023). However, this process was inhibited by co-adsorbing of various species such as SO_2 and H_2O, which competed for active sites, as evidenced by the weakening of infrared spectral bands for TMA and its derivatives in Section 3.2. In Pathway 1 (O_2-initiated, N-attack), the N atom of adsorbed TMA was attacked by the oxidation of O_2 (Atkinson and Pitts, 1978), forming $(CH_3)_3NO$. According to DFT calculations, in the presence of oxidants, $(CH_3)_3NO$ was readily decomposed to CH_3NO_2, which was a highly exothermic step (ΔE=−114.58 kcal/mol). This was experimentally corroborated by the significant increase in $\nu_{as}(NO_2)$ band at 1580 cm^{-1} (assigned to CH_3NO_2) following the introduction of NO_2. Additionally, $(CH_3)_3NO$ underwent intramolecular H-transfer to form $(CH_3)_2CH_2NOH$, which was subsequently oxidized to $CH_3N(OH)CHO$. However, the H-transfer step possessed a high energy barrier (ΔE=+15.69 kcal/mol), rendering this route kinetically less competitive. This is consistent with the phenomenon of fewer characteristic peaks for CH_3NO_2 and $(CH_3)_2CH_2NOH$, as described in Section 3.2.

In Pathway 2 (•OH-initiated, C-attack), •OH attacked C-H bond of a methyl group in TMA, generating $(CH_3)_2NCH_2$• radical. This radical rapidly reacted with O_2 to form a peroxy radical ($(CH_3)_2NCH_2OO$•), which was then converted to an alkoxy radical ($(CH_3)_2NCH_2O$•). The $(CH_3)_2NCH_2O$• radical followed two distinct routes (Ge et al., 2016): 1) the elimination of HCHO to produce $CH_3N{=}CH_2$ (ΔE=−25.06 kcal/mol); and 2) highly exothermic formation of $(CH_3)_2NCHO$ (ΔE=−117.48 kcal/mol). The latter route was strongly supported by the significant enhancement of ν_s(C=O) band at 1684 cm^{-1}, which was observed in the presence of NO_2 (Fig. 1b, E_3). Subsequently, $(CH_3)_2NCHO$ was further oxidized to HCOOH, which was consistent with the observed decrease in the band intensity of 1684 cm^{-1} and the concurrent increase in the intensity of δ(O-H) band at 1394 cm^{-1} under O_2 exposure. The subsequent fate of HCOOH bridged the interfacial and gas-phase chemistries. As demonstrated in Section 3.4, HCOOH was adsorbed by $Fe(NO_3)_3$, which promoted its photolysis to gener-

ate •CHO radicals. These radicals acted as key precursors that underwent C-C coupling reactions with CH_3 radicals to produce CH_3CHO and CH_3COOH (Wang et al., 2021; Zhang et al., 2023). Moreover, CH_3OH was likely formed through the reaction between CH_3 and •OH (Srinivasan et al., 2007; Vasudevan et al., 2008).

Through a synergistic approach combining DRIFTs, PTR-TOF-MS, and DFT calculations, the present study elucidates a novel C-attack-dominated mechanism for the formation of CH_3OH, CH_3CHO, and CH_3COOH during the reaction of TMA on Fe_2O_3/$Fe(NO_3)_3$ particles. This mechanism is driven by the unique interfacial properties of the proposed catalyst and stands in contrast to previously established N-attack pathways. More specifically, Fe^{3+} Lewis acid sites, along with interfacial ROSs (O_{ads}/O_{latt}), synergistically polarize the C-H bonds in TMA (Wang and Wang, 2018; Wang et al., 2025), making them highly susceptible to nucleophilic attack by ·OH radicals (contrasting with the N-attack pathway driven by electrophilic O_3 (Ge et al., 2016). Furthermore, DFT calculations confirm the thermodynamic dominance of this C-attack (Pathway 2), showing the formation of $(CH_3)_2NCHO$ and its subsequent oxidation to HCOOH/CH_3CHO, which is highly exothermic (ΔE=−117.48 kcal/mol). This theoretical finding is strongly corroborated by quantification conducted using PTR-TOF-MS, which identifies CH_3CHO as the principal gas-phase product, accounting for 48 % of the total yield and thus explaining its high concentration.

4. Conclusions

The present study elucidated the impacts of environment factors (NO_2, O_2, SO_2, H_2O, and light) and properties of particles on the products of TMA's heterogenous reaction on Fe_2O_3/$Fe(NO_3)_3$ particles by using a combined approach of DRIFTs, PTR-TOF-MS, and theoretical simulations. Nitrous oxide (NO_2) enhanced the consumption of TMA and promoted the formation of specific derivatives, while O_2 favored the production of more highly oxidized compounds. In contrast, SO_2 and H_2O inhibited the reaction through competitive adsorption for active sites. A powerful synergistic effect between light and complex gas mixtures was observed that accelerated the conversion of TMA and the oxidative removal of SO_2/H_2O. Additionally, Fe_2O_3 served as the primary reactive interface for TMA, while $Fe(NO_3)_3$ acted as a key photochemical promoter by providing an additional source of •OH. However, reduction in the size of Fe_2O_3 particles and increased amount of $Fe(NO_3)_3$ adversely affected both the structure of particles and the active sites. Crucially, the composite material of Fe_2O_3/$Fe(NO_3)_3$ was far more reactive than a simple physical mixture of individual components. Mechanistic analysis provided a comprehensive framework connecting the interfacial and gas-phase chemistries. It should be noted that the fixed concentrations of complex gas mixtures limited the extrapolation of our findings to dynamic environmental scenarios. Future work should employ online dynamic dilution systems to precisely control gas concentration gradients simulating atmospheric variability. This work provides critical insights into the heterogeneous chemistry of OAs on mineral particles in atmosphere, with significant implications for the formation of secondary organic aerosols and atmospheric nitrogen cycling.

CRediT authorship contribution statement

Chenxu Gao: Writing – original draft, Methodology, Investigation. **Cheng Chen:** Writing – original draft, Formal analysis. **Jiangyao Chen:** Writing – review & editing, Writing – original draft, Validation, Supervision, Conceptualization.

Declaration of competing interest

The authors declare that they have no known competing financial interests or personal relationships that could have appeared to influence the work reported in this paper.

Acknowledgments

This work was supported by the National Natural Science Foundation of China (Nos. 42177354 and 42577424) and Guangzhou Basic and Applied Basic Research Scheme (No. 2024A04J6358).

Appendix A Supplementary data

Supplementary material associated with this article can be found in the online version at doi:10.1016/j.jes.2026.01.012.

References

Arathala, P., Musah, R.A., 2021. Catalytic effect of water and formic acid on the reaction of carbonyl sulfide with dimethyl amine under tropospheric conditions. Phys. Chem. Chem. Phys. 23 (14), 8752–8766.

Atkinson, R., Pitts, J.N.J., 1978. Kinetics of the reactions of O(^{3}P) atoms with the amines CH_3NH_2, $C_2H_5NH_2$, $(CH_3)_2NH$, and $(CH_3)_3N$ over the temperature range 298-440 K. J. Chem. Phys. 68 (3), 911–915.

Busca, G., Lamotte, J., Lavalley, J.C., Lorenzelli, V., 1987. FT-IR study of the adsorption and transformation of formaldehyde on oxide surfaces. J. Am. Chem. Soc. 109 (17), 5197–5202.

Cano-Casanova, L., Amorós-Pérez, A., Lillo-Ródenas, M.A., Román-Martínez, M.D., 2018. Effect of the preparation method (sol-gel or hydrothermal) and conditions on the TiO_2 properties and activity for propene oxidation. Materials 11 (11), 2227.

Cao, J.Y., Qiu, X.H., Gao, J., Wang, F.Y., Wang, J.B., Wu, J., et al., 2021. Significant decrease in SO_2 emission and enhanced atmospheric oxidation trigger changes in sulfate formation pathways in China during 2008-2016. J. Cleaner Prod. 326, 129396.

Cao, W., Tan, O.K., Pan, J.S., Zhu, W., Reddy, C.V.G., 2002. XPS characterization of xα-Fe_2O_3–(1-x)ZrO_2 for oxygen gas sensing application. Mater. Chem. Phys. 75 (1–3), 67–70.

Chebbi, A., Carlier, P., 1996. Carboxylic acids in the troposphere, occurrence, sources, and sinks: a review. Atmos. Environ. 30 (24), 4233–4249.

Chen, C.T., Zhao, C.H., Zhou, X., Chen, J.H., Chen, L.Y., Li, F.T.C., 2021. DFT study on the interaction of H_2O and O_2 with α-Fe_2O_3 (001) surface. Vacuum 188, 110164.

Chen, M.L., Yin, M.J., Su, Y.T., Li, R.Z., Liu, K.Z., Wu, Z.B., et al., 2023. Atmospheric heterogeneous reaction of chlorobenzene on mineral α-Fe_2O_3 particulates: a chamber experiment study. Front. Env. Sci. Eng. 17 (11), 134.

Chen, Y., Tian, M., Huang, R.J., Shi, G.M., Wang, H.B., Peng, C., et al., 2019. Characterization of urban amine-containing particles in southwestern China: seasonal variation, source, and processing. Atmos. Chem. Phys. 19 (5), 3245–3255.

Cheng, X.M., Li, K.Z., Wei, Y.G., Zhu, X., Tian, D., 2017. Modification of KNO_3 on the reducibility and reactivity of Fe_2O_3-based oxygen carriers for chemical-looping combustion of methane. Can. J. Chem. Eng. 95 (8), 1569–1578.

Chu, B.W., Wang, Y.L., Yang, W.W., Ma, J.Z., Ma, Q.X., Zhang, P., et al., 2019. Effects of NO_2 and C_3H_6 on the heterogeneous oxidation of SO_2 on TiO_2 in the presence or absence of UV–Vis irradiation. Atmos. Chem. Phys. 19 (23), 14777–14790.

Chu, B.W., Zhang, X., Liu, Y.C., He, H., Sun, Y., Jiang, J.K., et al., 2016. Synergetic formation of secondary inorganic and organic aerosol: effect of SO_2 and NH_3 on particle formation and growth. Atmos. Chem. Phys. 16 (22), 14219–14230.

Chung, K.C., Quon, J.E., 1973. Capacity of ferric oxide particles to oxidize sulfur dioxide in air. Environ. Sci. Technol. 7 (6), 532–538.

Dong, L., Liu, Z., Hu, Y.H., Xu, B., Chen, Y., 1998. Dispersion and reduction behavior of CuO/α-Fe_2O_3 systems. J. Saudi Chem. Soc. 94 (19), 3033–3038.

Du, X.R., Huang, Y.K., Pan, X.L., Han, B., Su, Y., Jiang, Q.K., et al., 2020. Size-dependent strong metal-support interaction in TiO_2 supported Au nanocatalysts. Nat. Commun. 11 (1), 8.

Duporte, G., Parshintsev, J., Barreira, L.M.F., Hartonen, K., Kulmala, M., Riekkola, M.L., 2016. Nitrogen-containing low volatile compounds from pinonaldehyde-dimethylamine reaction in the atmosphere: a laboratory and field study. Environ. Sci. Technol. 50 (9), 4693–4700.

Durgaprasad, G., Sathyanarayana, D.N., Patel, C.C., Randhawa, H.S., Goel, A., Rao, C.N.R., 1972. Normal vibrations of N,N-dimethylacetamide. Spectrochim. Acta A 28 (12), 2311–2318.

Gai, Y.B., Ge, M.F., Wang, W.G., 2010. Rate constants for the gas phase reactions of ozone with diethylamine and triethylamine. Acta Phys. Chim. Sin. 26 (7), 1768–1772.

Gao, X.Y., Zhu, M.L., Long, Y., Zhang, X.J., Min, D.D., 2024. Heterogeneous reaction of NO_2 with hematite: the effects of UV irradiation, O_2 and relative humidity. Spectrochim. Acta A 314, 124205.

Ge, Y.L., Liu, Y.C., Chu, B.W., He, H., Chen, T.Z., Wang, S.X., et al., 2016. Ozonolysis of trimethylamine exchanged with typical ammonium salts in the particle phase. Environ. Sci. Technol. 50 (20), 11076–11084.

Ge, X.L., Wexler, A.S., Clegg, S.L., 2011. Atmospheric amines - part I. A review. Atmos. Environ. 45 (3), 524–546.

Gen, M.S., Zhang, R.F., Huang, D.D., Li, Y.J., Chan, C.K., 2019. Heterogeneous SO_2 oxidation in sulfate formation by photolysis of particulate nitrate. Environ. Sci. Technol. Lett. 6 (2), 86–91.

Ginoux, P., Prospero, J.M., Gill, T.E., Hsu, N.C., Zhao, M., 2012. Global-scale attribution of anthropogenic and natural dust sources and their emission rates based on MODIS Deep Blue aerosol products. Rev. Geophys. 50 (3), 1–36.

Golay, Z.M., Jones, S.H., Donaldson, D.J., 2022. Reactive uptake of gas-phase NO_2 by urban road dust in the dark. ACS Earth Space Chem. 6 (11), 2666–2672.

Grassian, V.H., 2001. Heterogeneous uptake and reaction of nitrogen oxides and volatile organic compounds on the surface of atmospheric particles including oxides, carbonates, soot and mineral dust: implications for the chemical balance of the troposphere. Int. Rev. Phys. Chem. 20 (3), 467–548.
Guan, C., Li, X.L., Luo, Y.Q., Huang, Z., 2014. Heterogeneous reaction of NO_2 on α-Al_2O_3 in the dark and simulated sunlight. J. Phys. Chem. A 118 (34), 6999–7006.
Gurajala, D., Sathyanarayana, D.N., Patel, C.C., 1971. Infrared spectra and normal vibrations of N,N-dimethylformamide and N,N-dimethylthioformamide. Bull. Chem. Soc. Jpn. 44 (2), 316–322.
He, G.Z., He, H., 2020. Water promotes the oxidation of SO_2 by O_2 over carbonaceous aerosols. Environ. Sci. Technol. 54 (12), 7070–7077.
Helali, S., Puzenat, E., Perol, N., Safi, M.J., Guillard, C., 2011. Methylamine and dimethylamine photocatalytic degradation-adsorption isotherms and kinetics. Appl. Catal. A–Gen. 402 (1–2), 201–207.
Hoque, M.M.M., Kawamura, K., 2016. Longitudinal distributions of dicarboxylic acids, ω-oxoacids, pyruvic acid, α-dicarbonyls, and fatty acids in the marine aerosols from the central Pacific including equatorial upwelling. Glob. Biogeochem. Cycle 30 (3), 534–548.
Huang, S., Feng, F., Huang, R.T., Ouyang, T., Liu, J.L., Liu, Z.Q., 2022a. Activating C–H bonds by tuning Fe sites and an interfacial effect for enhanced methanol oxidation. Adv. Mater. 34 (50), 2208438.
Huang, S., Song, Q.C., Hu, W.W., Yuan, B., Liu, J.W., Jiang, B., et al., 2022b. Chemical composition and sources of amines in $PM_{2.5}$ in an urban site of PRD, China. Environ. Res. 212, 113261.
Kim, C., Chae, S., Park, Y., Choi, W., 2021. Synergistic coupling of Fe_2O_3 and carbon paper that enables photocatalytic mineralization of organic contaminants in the absence of chemical oxidants under visible light. ACS ES&T Eng. 2 (2), 232–241.
Levenspiel, O., 1972. Chemical reaction engineering. Ind. Eng. Chem. Res. 38 (11), 4140–4143.
Li, H., Wang, X.D., Li, W.H., Wang, X.M., Cheng, R.J., He, D.F., et al., 2024. Efficient synthesis of amides from secondary alcohols and CH_3CN promoted by $Fe(NO_3)_3{\cdot}9H_2O$. RSC Adv. 14 (40), 29588–29594.
Li, L., Chen, Z.M., Zhang, Y.H., Zhu, T., Li, J.L., Ding, J., 2006. Kinetics and mechanism of heterogeneous oxidation of sulfur dioxide by ozone on surface of calcium carbonate. Atmos. Chem. Phys. 6 (1), 125–139.
Li, L.J., Hoffmann, M.R., Colussi, A.J., 2018. Role of nitrogen dioxide in the production of sulfate during Chinese haze-aerosol episodes. Environ. Sci. Technol. 52 (5), 2686–2693.
Li, X., Liu, C.Y., Wu, D.Y., Li, J.Z., Huo, P.W., Wang, H.Q., 2019. Improved charge transfer by size-dependent plasmonic Au on C_3N_4 for efficient photocatalytic oxidation of RhB and CO_2 reduction. Chin. J. Catal. 40 (6), 928–939.
Li, Y., Shao, M., Lu, S.H., Chang, C.C., Dasgupta, P.K., 2010. Variations and sources of ambient formaldehyde for the 2008 Beijing Olympic games. Atmos. Environ. 44 (21–22), 2632–2639.
Lien, C.F., Lin, Y.F., Lin, Y.S., Chen, M.T., Lin, J.L., 2005. FTIR study of adsorption and surface reactions of $N(CH_3)_3$ on TiO_2. J. Phys. Chem. B 109 (21), 10962–10968.
Ling, Y.J., Chen, J., Min, F.F., Cheng, Y.L., Chu, X.X., Shang, H.H., et al., 2023. Influence mechanism of Fe(II/III) doping on the adsorption of methylamine salts on kaolinite surfaces elucidated through DFT calculations. J. Mol. Liq. 390, 123082 Pt.B.
Liu, C., Ma, Q.X., Liu, Y.C., Ma, J.Z., He, H., 2012. Synergistic reaction between SO_2 and NO_2 on mineral oxides: a potential formation pathway of sulfate aerosol. Phys. Chem. Chem. Phys. 14 (5), 1668–1676.
Liu, F.X., Bi, X.H., Zhang, G.H., Peng, L., Lian, X.F., Lu, H.Y., et al., 2017. Concentration, size distribution and dry deposition of amines in atmospheric particles of urban Guangzhou, China. Atmos. Environ. 171, 279–288.
Liu, S.X., Yu, B., Wang, S., Shen, Y.Q., Cong, H.L., 2020. Preparation, surface functionalization and application of Fe_3O_4 magnetic nanoparticles. Adv. Colloid Interface Sci. 281, 102165.
Liu, Z.Y., Li, M., Wang, X.F., Liang, Y.H., Jiang, Y.R., Chen, J., et al., 2022. Large contributions of anthropogenic sources to amines in fine particles at a coastal area in northern China in winter. Sci. Total Environ. 839, 156281.
Ma, T., Niuhe, J., Lu, S.L., Zhang, L., Zhou, S.M., Liu, J., et al., 2023. Comparison of the heterogeneous reaction of NO_2 on the surface of clay minerals and desert dust particles. Environ. Pollut. 334, 122134.
Pettersson, M., Lundell, J., Khriachtchev, L., Räsänen, M., 1997. IR spectrum of the other rotamer of formic acid, cis-HCOOH. J. Am. Chem. Soc. 119 (48), 11715–11716.
Mu, Y., Ai, Z.H., Zhang, L.Z., 2017. Phosphate shifted oxygen reduction pathway on $Fe@Fe_2O_3$ core-Shell nanowires for enhanced reactive oxygen species generation and aerobic 4-chlorophenol degradation. Environ. Sci. Technol. 51 (14), 8101–8109.
Murphy, W.F., Zerbetto, F., Duncan, J.L., Mckean, D.C., 1993. Vibrational spectrum and harmonic force field of trimethylamine. J. Phys. Chem. 97, 581–595.
Niu, Z.Z., Kong, S.F., Zheng, H., Yan, Q., Liu, J.H., Feng, Y.K., et al., 2021. Temperature dependence of source profiles for volatile organic compounds from typical volatile emission sources. Sci. Total Environ. 751, 141741.
Place, B.K., Quilty, A.T., Di Lorenzo, R.A., Ziegler, S.E., Vandenboer, T.C., 2017. Quantitation of 11 alkylamines in atmospheric samples: separating structural isomers by ion chromatography. Atmos. Meas. Tech. 10 (3), 1061–1078.
Sha, Q.E., Zhu, M.N., Huang, H.W., Wang, Y.Z., Huang, Z.J., Zhang, X.C., et al., 2021. A newly integrated dataset of volatile organic compounds (VOCs) source profiles and implications for the future development of VOCs profiles in China. Sci. Total Environ. 793, 148348.
Shen, X.L., Chen, J.Y., Li, G.Y., An, T.C., 2023. A new advance in the pollution profile, transformation process, and contribution to aerosol formation and aging of atmospheric amines. Environ. Sci. Atmos. 3 (3), 444–473.
Sorooshian, A., Murphy, S.N., Hersey, S., Gates, H., Padro, L.T., Nenes, A., et al., 2008. Comprehensive airborne characterization of aerosol from a major bovine source. Atmos. Chem. Phys. 8 (17), 5489–5520.
Srinivasan, N.K., Su, M.C., Michael, J.V., 2007. High-temperature rate constants for $CH_3OH+Kr \rightarrow$ products, $OH+CH_3OH \rightarrow$ products, $OH+(CH_3)_2CO \rightarrow CH_2COCH_3+H_2O$, and $OH+CH_3 \rightarrow CH_2+H_2O$. J. Phys. Chem. A 111 (19), 3951–3958.
Styler, S.A., Donaldson, D.J., 2012. Heterogeneous photochemistry of oxalic acid on Mauritanian sand and Icelandic volcanic ash. Environ. Sci. Technol. 46 (16), 8756–8763.
Sugrañez, R., Balbuena, J., Cruz-Yusta, M., Martin, F., Morales, J., Sánchez, L., 2015. Efficient behaviour of hematite towards the photocatalytic degradation of NO_x gases. Appl. Catal. B Environ. 165, 529–536.
Taylor, W.D., Allston, T.D., Moscato, M.J., Fazekas, G.B., Kozlowski, R., Takacs, G.A., 1980. Atmospheric photodissociation lifetimes for nitromethane, methyl nitrite, and methyl nitrate. Int. J. Chem. Kinet. 12 (4), 231–240.
Tercero Espinoza, L.A., Neamtu, M., Frimmel, F.H., 2007. The effect of nitrate, Fe(III) and bicarbonate on the degradation of bisphenol A by simulated solar UV-irradiation. Water Res. 41 (19), 4479–4487.
Urone, P., Lutsep, H., Noyes, C.M., Parcher, J.F., 1968. Static studies of sulfur dioxide reactions in air. Environ. Sci. Technol. 2 (8), 13–19.
Usher, C.R., Al-Hosney, H., Carlos-Cuellar, S., Grassian, V.H., 2002. A laboratory study of the heterogeneous uptake and oxidation of sulfur dioxide on mineral dust particles. J. Geophys. Res. Atmos. 107 (D23), 1–9.
Usher, C.R., Michel, A.E., Grassian, V.H., 2003. Reactions on mineral dust. Chem. Rev. 103 (12), 4883–4939.
Vasudevan, V., Cook, R.D., Hanson, R.K., Bowman, C.T., Golden, D.M., 2008. High-temperature shock tube study of the reactions $CH_3+OH \rightarrow$ products and $CH_3OH+Ar \rightarrow$ products. Int. J. Chem. Kinet. 40 (8), 488–495.
Wang, H., Huang, B., Chang, Y.C., Ding, Y., Qu, Z.P., 2025. Accelerating HCHO-to-CO_2 conversion of a zeolite-Ag tandem catalyst via adjusting metal-oxygen lewis pairs. ACS Catal. 15 (8), 6239–6247.
Wang, H.C., Wang, H.L., Lu, X., Lu, K.D., Zhang, L., Tham, Y.J., et al., 2023. Increased night-time oxidation over China despite widespread decrease across the globe. Nat. Geosci. 16 (3), 217–223.
Wang, J., Wang, G.C., 2018. Promotion effect of methane activation on Cu(111) by the surface-active oxygen species: a combination of DFT and reaxff study. J. Phys. Chem. C 122 (30), 17338–17346.
Wang, Q.Y., Yeung, K.L., Bañares, M.A., 2020. Ceria and its related materials for VOC catalytic combustion: a review. Catal. Today 356, 141–154.
Wang, R.X., Yang, N., Li, J.L., Xu, L., Tsona, N.T., Du, L., et al., 2022. Heterogeneous reaction of SO_2 on $CaCO_3$ particles: different impacts of NO_2 and acetic acid on the sulfite and sulfate formation. J. Environ. Sci. 114, 149–159.
Wang, X.L., Ramírez, P.J., Liao, W.J., Rodriguez, J.A., Liu, P., 2021. Cesium-induced active sites for C–C coupling and ethanol synthesis from CO_2 hydrogenation on Cu/ZnO $(000\bar{1})$ surfaces. J. Am. Chem. Soc. 143 (33), 13103–13112.
Wollenhaupt, M., Crowley, J.N., 2000. Kinetic studies of the reactions $CH_3 + NO_2 \rightarrow$ products, $CH_3O + NO_2 \rightarrow$ products, and $OH + CH_3C(O)CH_3 \rightarrow CH_3C(O)OH + CH_3$, over a range of temperature and pressure. J. Phys. Chem. A 104 (27), 6429–6438.
Wu, L.Y., Tong, S.R., Zhou, L., Wang, W.G., Ge, M.F., 2013. Synergistic effects between SO_2 and HCOOH on α-Fe_2O_3. J. Phys. Chem. A 117 (19), 3972–3979.
Xu, B.Y., Shang, J., Zhu, T., Tang, X.Y., 2011. Heterogeneous reaction of formaldehyde on the surface of γ-Al_2O_3 particles. Atmos. Environ. 45 (21), 3569–3575.
Xu, W.Q., Yu, Y.B., Zhang, C.B., He, H., 2008. Selective catalytic reduction of NO by NH_3 over a Ce/TiO_2 catalyst. Catal. Commun. 9 (6), 1453–1457.
Yang, N., Tsona, N.T., Cheng, S.M., Li, S.Y., Xu, L., Wang, Y.F., et al., 2020. Competitive reactions of SO_2 and acetic acid on α-Al_2O_3 and $CaCO_3$ particles. Sci. Total Environ. 699, 134362.
Yang, W.W., Gong, J., Wang, X., Bao, Z.H., Guo, Y.B., Wu, Z.L., 2021. A review on the impact of SO2 on the oxidation of NO, hydrocarbons, and CO in diesel emission control catalysis. ACS Catal. 11 (20), 12446–12468.
Zhang, S.Q., Kong, L.D., Zhao, X., Jansen, R., Chen, J.M., 2013. Effects of ammonia and amines on heterogeneous oxidation of carbonyl sulfide on hematite. Acta Phys. Chim. Sin. 29 (9), 2027–2034.
Zhang, W.Q., Xi, D.W., Chen, Y.H., Chen, A.B., Jiang, Y.W., Liu, H.J., et al., 2023. Light–driven flow synthesis of acetic acid from methane with chemical looping. Nat. Commun. 14 (1), 3047.
Zhao, Q., Zheng, Y.F., Song, C.F., Liu, Q.L., Ji, N., Ma, D.G., et al., 2020. Novel monolithic catalysts derived from in-situ decoration of Co_3O_4 and hierarchicalCo_3O_4@MnOx on Ni foam for VOC oxidation. Appl. Catal. B Environ. 265, 118552.
Zheng, F., Dong, F.Q., Zhou, L., Chen, Y.Z., Yu, J.Y., Luo, X.J., et al., 2022. Research progress on heterogeneous reactions of pollutant gases on the surface of atmospheric mineral particulate matter in china. Atmos. Ocean 13 (8), 1283.